applied optics

Thermally induced bias error due to strain inhomogeneity through the fiber optic gyroscope coil

Berk Osunluk,[1,2,*] Serdar Ogut,[1,3] and Ekmel Ozbay[1,3]

[1]Department of Electrical and Electronics Engineering, Bilkent University, Ankara 06800, Turkey
[2]Microelectronics, Guidance and Electro-optics Sector, Aselsan Inc., Ankara 06011, Turkey
[3]Nanotechnology Research Center—NANOTAM, Bilkent University, Ankara 06800, Turkey
*Corresponding author: berk.osunluk@bilkent.edu.tr

Received 20 August 2020; revised 18 October 2020; accepted 19 October 2020; posted 21 October 2020 (Doc. ID 406045); published 17 November 2020

One of the performance limits of a navigation grade fiber optic gyroscope is the bias error due to the thermal sensitivity of the fiber coil. Thermal stress inside the fiber coil is an important source of the bias error. The reduction of the total stress inside the fiber coil can be limited. In this paper, it is shown that further improvement can be achieved by controlling the strain inhomogeneity through the fiber coil. A validated simulation environment is presented for strain distribution analysis. Thermally induced bias error formation mechanisms are compared. The effect of the strain inhomogeneity is reduced by presenting a different coil cross section and spool material. Experiments utilizing a coil design with better performance are presented for the verification of the approach.

https://doi.org/10.1364/AO.406045

1. INTRODUCTION

A fiber optic gyroscope (FOG) is a high-performance angular rotation rate measurement sensor that is widely used for navigation, positioning, and stabilization [1]. One of the main limits for FOG performance is the thermally induced bias error. The thermal sensitivity of the fiber coil is defined by [2]. Elasto-optical interactions are shown to be another error source for a thermally induced phase error [3]. The reduction of the thermally induced bias error is still being discussed in the literature. Literature works include thermal modeling of the fiber coil [4,5], fiber technologies with low thermal sensitivity [6], and winding methods [7,8]. There are also several works that indicate the relation between the stress/strain and the bias error and they try to reduce the total stress/strain as a whole [9,10].

In the present paper, we discuss the reduction of the bias error by controlling the strain distribution through the fiber coil, although the total stress is not reduced. Strain distributions are obtained by simulations of a thermal model that is discussed and validated in our previous work [11]. The validated simulation environment is important for further analysis of the bias error mechanisms that cannot be measured easily in the laboratory. In this paper, the model in [11] is handled as Coil Design #1 and used for detailed bias error, von Mises stress and strain inhomogeneity analyses. Bias error can be separated into the pure Shupe error and the elasto-optical error. The simulations show that the elasto-optical error is greater than the pure Shupe error. Second, the elasto-optical error can be separated into the error due to elongation and due to a refractive index change. We show that elongation is the dominant one. The homogeneity of the strain of each fiber segment through the fiber coil is important as well as the total strain change with respect to temperature. Strain homogeneity is separated into axial and radial inhomogeneity. Changes in the von Mises stress and the strain inhomogeneity distribution for different spool configurations for Coil Design #1 are presented. Axial and radial homogeneity depends on the fiber cross-section geometry and the spool design. The simulations of three coil designs are discussed in terms of bias error reduction. A fiber optic gyroscope coil is produced with the proposed coil design parameters and tested in the laboratory. Consistent test results verify the effectiveness of the approach. Theoretical and experimental results are reported as 0.319 and 0.435 (°h)/(°C/min), respectively for a 1.1 km length and 8 cm diameter quadrupole fiber coil. These results show that the approach proposes simple design changes to increase the performance to the same order of magnitude of the latest developments in the literature, better than various quadrupole designs [12–14] and close to octupolar winding performance [13,14].

2. THEORETICAL BACKGROUND

Thermal fluctuations create nonreciprocal phase shifts between counterpropagating waves in the fiber coil. Bias error due to nonreciprocal phase shift is defined by [2]

$$\Omega_S(t) = \frac{n}{LD}\frac{\partial n}{\partial T}\int_0^L \dot{T}(s,t)(L-2s)\mathrm{d}s, \quad (1)$$

where L is the length of the fiber, D is the diameter of the fiber coil, n is the refractive index of the fiber core, $\partial n/\partial T$ is the temperature coefficient of n, $\dot{T}(s,t)$ is the temperature field time derivative, and s is the fiber portion where the temperature fluctuates. This error is called the pure Shupe error, as the main mechanism is the change of the temperature.

Reference [3] extends this analysis for elasto-optical interactions, given in Eq. (2). Strain change due to temperature or stress results in a phase shift on the fiber segment ds which is integrated through the fiber coil:

$$\Omega_{\mathrm{EO}}(t) = \frac{n}{LD}\int_0^L \left[A\dot{\varepsilon}_f(\mathrm{s},\mathrm{t}) - \mathrm{B}\dot{\varepsilon}_p(\mathrm{s},\mathrm{t})\right](L-2s)\mathrm{d}s, \quad (2)$$

where $A = \mathrm{n}(1-\frac{n^2}{2}p_{12})$, $B = \frac{n^3}{2}(p_{11}+p_{12})$, p_{12} and p_{11} are the photoelastic coefficients of the fiber glass, and $\dot{\varepsilon}_f$ and $\dot{\varepsilon}_p$ are the time derivatives of the strain fields through the fiber propagation axis and the perpendicular axis inside the fiber core, respectively. The strain change can be induced by the temperature fluctuation [9–14], the vibration [15], or the change of the moisture level inside the fiber [16]. The two bias error mechanisms are additive and the total bias error is

$$\Omega_{\mathrm{Total}} = \Omega_{\mathrm{EO}} + \Omega_S. \quad (3)$$

The term $(L-2s)$ in both Eqs. (1) and (2) describe that the bias error arises if the temperature/strain changes with respect to time, and the change is inhomogeneous. The bias error on the symmetric fiber segments s and $L-s$ cancels each other if they experience the same temperature/strain change. The symmetric winding methods (dipole, quadrupole, or octupole patterns [7,8]) purposed to locate the symmetric fiber segments as close as possible. The fiber segments cannot be placed exactly in the same location so the symmetry can be achieved to some extent and the bias error can be reduced only to a degree. Temperature/strain change should be as small as, and the distribution should be as homogeneous as possible for further improvement. The inhomogeneity is reduced into two dimensions and discretized in Section 4, while Eq. (2) formulates the effect of the strain homogeneity in three dimensions. The change and symmetry of the strain distribution are investigated separately for the two dimensions of the fiber coil, radial and axial.

3. MODELING OF THE FIBER COIL

In our previous work [11], we presented a finite element method (FEM) model for thermally induced rate errors for a fiber optic gyroscope coil. Modeling is based on three steps. The first step is to create a representative volume element with high-resolution mesh and obtain a homogeneous composite material representing the fiber coil, which is a transversely isotropic structure.

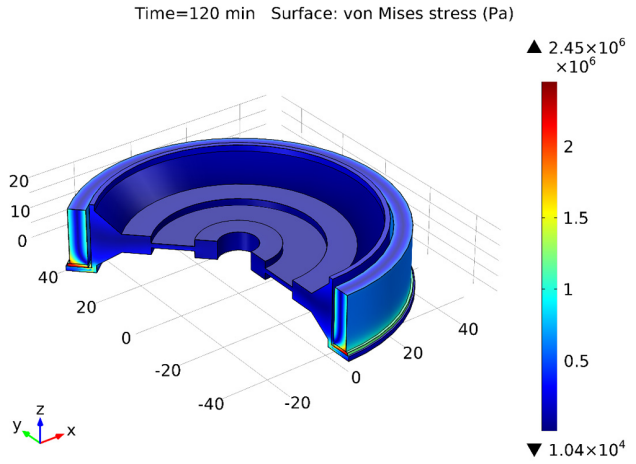

Fig. 1. FEM simulation of the fiber coil model. Fiber coil dimensions are in mm. High-stress region is in the coil spool intersection [11].

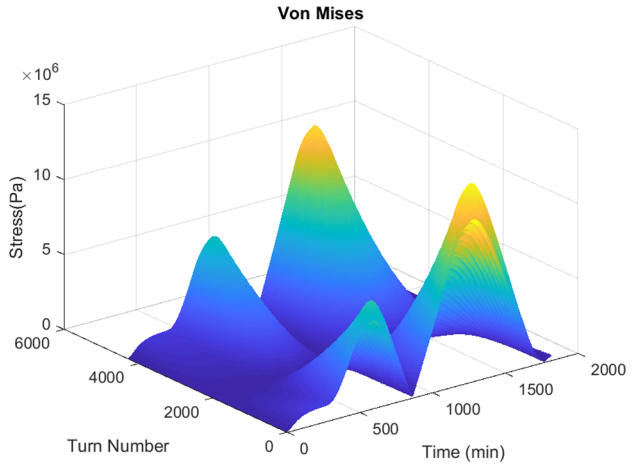

Fig. 2. Stress distribution through the fiber coil while the temperature is changing.

A second simulation provides the temperature, the stress, and strain change due to temperature fluctuations, and strain distributions on the fiber coil which is wounded on a spool together with air surrounding the coil and lastly a heat source encapsulating the air (Fig. 1). We verified the simulation environment with the experimental results of three fiber coils. We concluded that the elasto-optic effect is much stronger than the pure Shupe error for that coil design.

Figure 1 shows the von Mises stress distribution through the model for a time instant of the simulation. The highest stress is located in the intersection area of the fiber coil, which is modeled as a homogeneous composite material, and the spool. Different thermal expansion coefficients of the materials result in a high stress in the intersection area. Figure 2 shows the von Mises stress distribution for each fiber turn with respect to time. Temperature changes as time progresses and the von Mises stress increases dramatically for the highest and lowest turn numbers, which are located in the intersection area. In order to analyze the effect of the stress, we designed a new fiber coil without a spool

Table 1. Von Mises Stress Values for Different Spool Materials

Spool Material	Maximum Von Mises Stress (Pa)	Average Von Mises Stress (Pa)
Aluminum	1.34×10^7	2.15×10^6
Titanium	1.32×10^7	2.14×10^6
No spool	1.31×10^7	2.14×10^6

and with a titanium spool. Stress values are obtained from the model and given in Table 1. Although the von Mises stress characteristics and values stay the same, the bias error is significantly reduced. The stress/strain inhomogeneity in the fiber coil and the bias error calculations are significant.

4. BIAS ERROR CALCULATION METHOD

Equations (1) and (2) are discretized and the distance of each turn is calculated using the quadrupole cross-section view (Fig. 3). Practical quadrupole winding has several major differences from the ideal quadrupole. First, the length and diameter of the turns differ in each layer of the fiber coil, which results in radial asymmetry. Second, the first turn of each layer is wound either clockwise or counterclockwise and the last turn vice versa. This is a practical solution for passing the fiber from a layer to the next one. This second difference creates an axial asymmetry. We note that the axial asymmetry is not negligible, especially under thermal stress.

The fiber coil is a cylindrical structure and the integral can be represented in radius, azimuth, and height (r, θ, z). The fiber coil consists of the fiber core, cladding, coating, and adhesive. Light travels only in the fiber core so that the integral is taken through the fiber core that is only continuous through azimuth and discrete for axial and radial directions. Equation (1) is reduced into two dimensions and discretized:

$$\Omega_S(t) = \frac{n}{\pi N} \sum_{i=1}^{N_r} \frac{1}{d_i^2} \sum_{j=1}^{N_a} \int_0^{2\pi} \frac{\partial n}{\partial T} \dot{T}(r_i, \theta, z_j, t)(L - 2s)\mathrm{d}\theta \Delta s, \tag{4}$$

where d_i is the diameter of each turn; N_r, N_a are the radial and axial layer numbers, respectively; and $N = N_r \times N_a$ is the total number of turns. Using the relation $\Delta s = \frac{L}{N} = \frac{\pi d_i N}{N} = \pi d_i$, and taking the integral over $d\theta$ results as

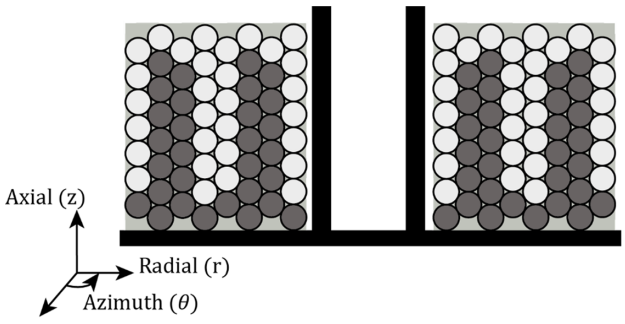

Fig. 3. Fiber coil cross-section view. The fiber coil winding has a quadrupole pattern, the fiber turn locations are orthocyclic, and the fiber is inside adhesive.

$$\Omega_S(t) = \frac{n}{N} \sum_{i=1}^{N_r} \frac{1}{d_i} \sum_{j=1}^{N_a} \frac{\partial n}{\partial T} \dot{T}(r_i, z_j, t)(L - 2s - l_i), \tag{5}$$

where l_i is the length of each fiber turn that is different for every radial layer. This equation is the two-dimension approximation for the calculation of the bias error due to temperature fluctuation.

We separated the elasto-optical error into two main sources: error due to the elongation of the fiber (Ω_{EOl}) and error due to refractive index change (Ω_{EOn}). Both of the error sources are discretized as in Eq. (4):

$$\Omega_{\mathrm{EO}}(t) = \Omega_{\mathrm{EOl}}(t) + \Omega_{\mathrm{EOn}}(t), \tag{6}$$

$$\Omega_{\mathrm{EOl}}(t) = \frac{n^2}{N} \sum_{i=1}^{N_r} \frac{1}{d_i} \sum_{j=1}^{N_a} \dot{\varepsilon}_f(r_i, z_j, t)(L - 2s - l_i), \tag{7}$$

$$\Omega_{\mathrm{EOn}}(t) = -\frac{n^4}{2N} \sum_{i=1}^{N_r} \frac{1}{d_i} \sum_{j=1}^{N_a} \big[p_{12}\dot{\varepsilon}_f(r_i, z_j, t) + (p_{11} + p_{12})\dot{\varepsilon}_p(r_i, z_j, t)\big](L - 2s - l_i). \tag{8}$$

5. SIMULATIONS

The simulation environment is a powerful tool to obtain information about the interactions that cannot be measured directly, inside the fiber coil, like strain distribution, a dominant bias error source, or thermal sensitivity. First, various bias error contributions of a model with the parameters of Coil Design #1 (Table 2) are obtained by simulations. Then, the strain inhomogeneity is presented for different spool types. Lastly, the simulations of two more coil designs are presented.

All simulations are run with an input temperature profile that spans a range from −40°C to +60°C while the temperature is increasing and then decreasing with a rate of 0.2°C/min. This profile reveals all of the temperature and temperature time derivative dependent errors in the interval.

A. Elongation Versus Refractive Index Change

The different error contributions of Coil Design #1 are shown in Table 3, wherein the pure Shupe error is much smaller than

Table 2. Coil Design Parameters

Parameter	Coil Design #1	Coil Design #2	Coil Design #3
Fiber length	1101 m	1101 m	1101 m
Number of winding layers	36	56	56
Number of loops per layer	106	77	77
Inner diameter of the coil	87 mm	73 mm	73 mm
Outer diameter of the coil	97.65 mm	89.53 mm	89.53 mm
Coil height	18.02 mm	13.09 mm	13.09 mm
Spool material	Aluminum	Aluminum	Titanium

Table 3. Error Contributions

Parameter $\left(\frac{^\circ/h}{^\circ C/min}\right)$	Coil Design #1	Coil Design #2	Coil Design #3
Shupe	0.0847	0.0790	0.0790
Elasto-optical (EO) error	2.62	1.06	−0.398
EO error due to refractive index change	−0.594	−0.273	0.110
EO error due to elongation	3.30	1.34	−0.508
Total	2.70	1.14	−0.319

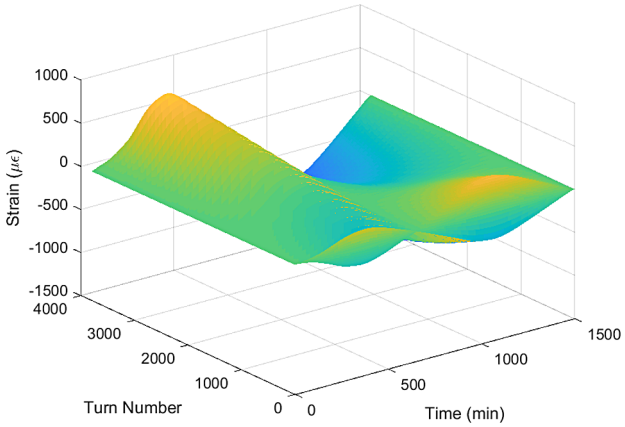

Fig. 4. Strain (through the fiber propagation axis) distribution with respect to time and the turn number. The temperature fluctuates as time progresses. The strain change rate is inhomogeneous [11].

the elasto-optical error. Second, the elongation of the fiber dominates the elasto-optical error. Although the error due to a refractive index change has a negative sign, it is not large enough to compensate for the error due to elongation. It is a significant conclusion that the strain through the fiber propagation axis is more significant than the perpendicular strain inside the fiber, so the change of the strain through the fiber propagation axis ($\dot{\varepsilon}_f$) should be reduced. We mainly deal with the strain through the fiber propagation axis, so it is hereinafter referred to as "strain."

B. Strain Inhomogeneity

Equation (7) shows that a fiber coil subjected to temperature fluctuation results in a gyroscope bias error if the strain through the fiber changes and the strain change rate is inhomogeneous. A simulation output, as shown in Fig. 4, shows the strain distribution through the fiber coil while the temperature is fluctuating. This strain field can be studied in two dimensions: the total strain change with respect to time, and the distribution of the strain change rate, i.e., the thermal expansion coefficient, for each fiber turn.

The integral through the fiber turn number gives the total strain in the fiber coil at each time interval. The total strain change with respect to temperature is plotted in Fig. 5(a). A fiber coil in the laboratory is subjected to a temperature change from −40°C up to +60°C and the flight time inside the fiber coil is measured continuously with an optical time-domain reflectometer (OTDR). The flight time includes the fiber refractive index change due to temperature which is compensated by using the coefficient. Refractive index change is found to be $7 \times 10^{-6}\ ^\circ C^{-1}$ which is close to the temperature coefficient of the refractive index for fiber core material, $10^{-5}\ ^\circ C^{-1}$.

Distribution of the strain change rate can be obtained by calculating the temperature coefficient for each fiber turn. Strain temperature coefficient versus turn location, as shown in Fig. 5(b), is a serrated line where the serration indicates the axial strain and the line indicates the radial strain. The strain coefficients of each turn in the same radius are averaged and named as the axial strain coefficients (α_a), and the brackets indicate averaging over all t. This gives the inhomogeneity in the fiber coil in the axial direction:

$$\alpha_a(z_j) = \frac{1}{N_r}\sum_{i=1}^{N_r}\langle \dot{\varepsilon}_f(r_i, z_j, t)\rangle. \tag{9}$$

A similar method is carried out in order to obtain the radial strain coefficients:

$$\alpha_r(r_i) = \frac{1}{N_a}\sum_{j=1}^{N_a}\langle \dot{\varepsilon}_f(r_i, z_j, t)\rangle. \tag{10}$$

Radial strain temperature coefficient change is a straight line, while the axial strain coefficients show an asymmetric characteristic (Fig. 6). A quadrupole pattern dictates the location of the fiber turns in order to be placed next to each other. Therefore, the symmetric strain distribution is important to reduce the total bias error. Although the value of the radial coefficient change is higher than the axial coefficient, the asymmetry of the axial distribution is the main bias error source. The asymmetric and rapid change in the axial coefficients of the inner layers results in a bias error, which is not compensated by the symmetric fiber turns.

The calculations for two other simulations of the fiber coil, with a titanium spool and without a spool cases, are shown in Fig. 6. The radial strain coefficients do not differ too much for different spool configurations. The axial strain coefficients are reduced, especially for the innermost layers. The titanium spool performs nearly as well as the no spool configuration.

The bias error contribution of the axial asymmetry can be reduced by changing the design of the fiber coil cross section. Coil design #2 has a fiber coil with a cross section that looks more like a square (Table 2) to balance the bias error contribution of the asymmetries (Fig. 7). The significant reduction in the axial strain coefficients reduces the bias error, although the asymmetry in the radial strain coefficient increases. The new coil design is smaller than the existing one. A better bias error performance is achieved, although the smaller coil results in a 12% reduction in the Sagnac scale factor (Table 3). Simulations show that the main bias error contribution is still the elasto-optical error due to elongation. The Shupe error stays nearly the same.

Further improvement can be achieved by changing the spool material. Aluminum is a widely used material because of its low cost and abundant usage in mechanical fabrication. Titanium is a more convenient material for high-performance fiber coil

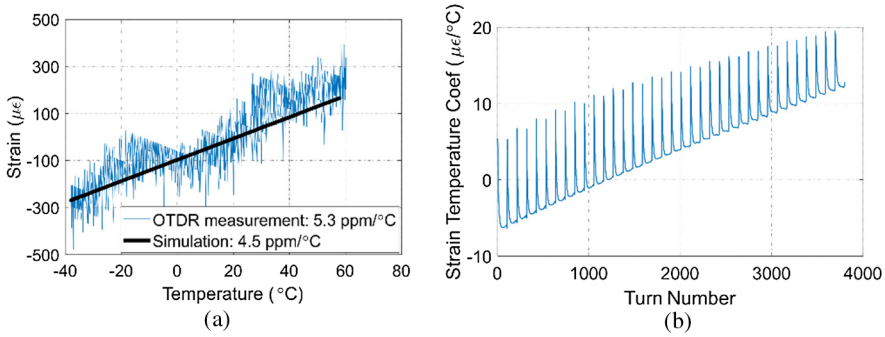

Fig. 5. (a) Total strain change of the fiber coil. Simulation output for each temperature point is compared with the OTDR measurement of a fiber coil. (b) Calculated strain temperature coefficient for each turn number.

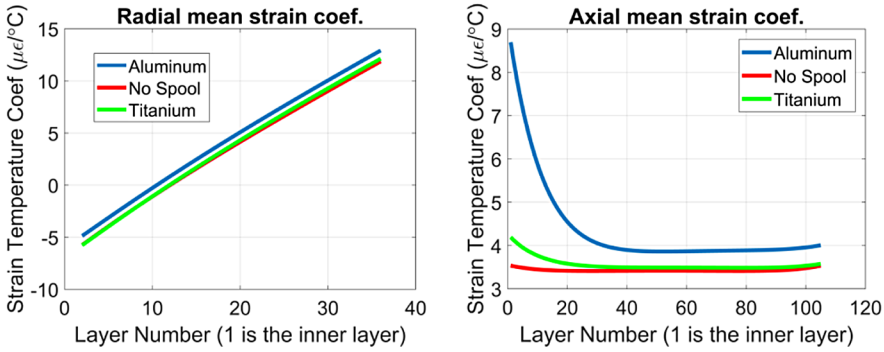

Fig. 6. Radial and axial mean strain temperature coefficients for different spool configurations.

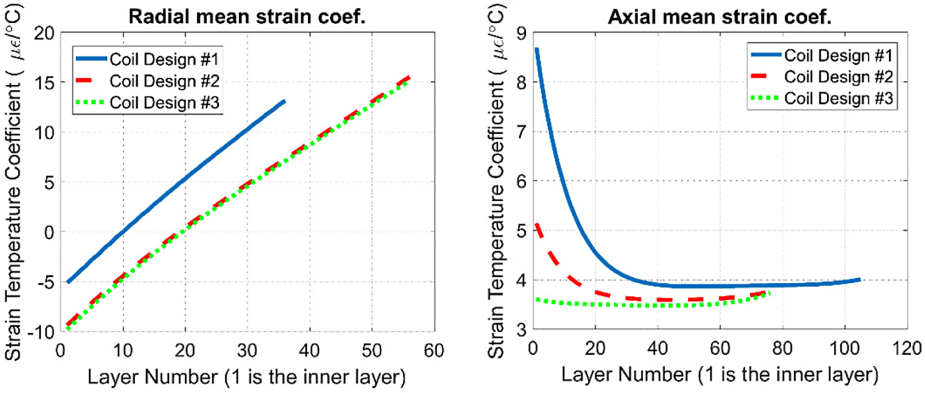

Fig. 7. Radial and axial mean strain temperature coefficients for Coil Designs #1, 2, and 3. Coil Designs #2 and 3 have more radial layers and fewer axial layers than Coil Design #1 (Table 2). Change in the spool material reduces the axial asymmetry while not affecting the radial signicantly.

design. The titanium thermal expansion coefficient is closer to the fiber itself than the aluminum. The third fiber coil design is presented with the same cross section as the second design but with a titanium spool (Table 2). Simulations show that the axial strain coefficient asymmetry is reduced without any significant change in the radial asymmetry (Fig. 7). The elasto-optical error is reduced more than sixfold relative to the first coil design, changes the sign, and becomes the inverse of the Shupe error (Table 3). The Shupe error stays nearly the same as in the second coil design. The Shupe error and the elasto-optical error cancel each other so that the total bias error is less than one-eighth of the first coil design.

6. EXPERIMENTS

A fiber coil is produced with the parameters of Coil Design #3 for the validation of the simulation outcomes. A closed-loop fiber optic gyroscope setup is built for the laboratory experiments. The setup consists of an amplified spontaneous emission light source, a multifunction integrated optics chip to apply square-wave phase modulation, an analog electronic board to amplify and sample the photodiode current and, lastly, a digital electronics board for the closed-loop operation. The setup is placed in a temperature chamber and a temperature profile ranging from -40°C to $+60^{\circ}$C with temperature rates

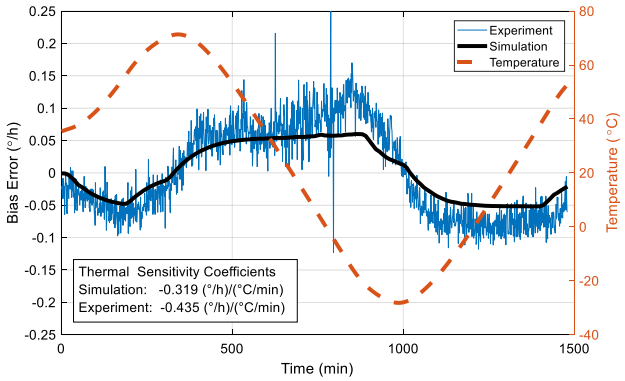

Fig. 8. Simulated and experimental bias error curves. Bias error correlates mostly with the time derivative of the temperature so that the thermal sensitivity of the fiber coil is calculated with respect to it.

of ±0.2°C/min is applied to the fiber coil. A temperature sensor is mounted on the fiber coil to collect the temperature data.

The mean value of the collected data is subtracted to eliminate the Earth rotation rate. One-minute averaging filter is applied to the data to filter out the gyroscope noise. Collected FOG data and the simulation results are plotted in Fig. 8 along with the calculated temperature sensitivity coefficients. The bias error characteristic of the FOG is shown to be highly consistent with the theoretical model.

7. CONCLUSIONS

In this paper, it is shown that the fiber optic gyroscope bias error under thermal fluctuation can be reduced by controlling the strain distribution through the fiber coil. Bias error can be decreased more than eightfold by reducing the strain inhomogeneity although the total stress on the fiber coil stays nearly the same. A validated simulation environment is a very useful tool for the analysis of the strain inhomogeneity through the fiber coil, which is an important parameter that cannot be measured directly. Lastly, two conclusions can be very useful for the thermal modeling of a fiber optic gyroscope coil: the elasto-optical error is the dominant effect relative to the pure Shupe error, and the bias error due to elongation is greater than the refractive index change.

Disclosures. The authors declare no conflicts of interest.

REFERENCES

1. H. C. Lefevre, *The Fiber-Optic Gyroscope*, 2nd ed. (Artech House, 2014).
2. D. M. Shupe, "Thermally induced non-reciprocity in the fiber optic interferometer," Appl. Opt. **19**, 654–655 (1980).
3. F. Mohr and F. Schadt, "Bias error in fiber optic gyroscopes due to elastooptic interactions in the sensor fiber," in *Second European Workshop on Optical Fibre Sensors*, Santander, Spain, 2004, pp. 410–413.
4. Z. Li, Z. Meng, T. Liu, and S. Yao, "A novel method for determining and improving the quality of a quadrupolar fiber gyro coil under temperature variations," Opt. Express **21**, 2521–2530 (2013).
5. Y. Zhang, Z. Gao, G. Wang, and W. Gao, "Modeling of thermal-induced rate error for FOG with temperature ranging from –40°C to 60°C," IEEE Photonics Technol. Lett. **26**, 18–21 (2014).
6. S. Bilin, H. K. Kim, M. J. F. Digonnet, and G. S. Kino, "Reduced thermal sensitivity of a fiber optic gyroscope using an air-core photonic bandgap fiber," J. Lightwave Technol. **25**, 861–865 (2007).
7. N. J. Frigo, "Compensation of linear sources of non-reciprocity in Sagnac interferometers," in *Fiber Optic and Laser Sensors I*, Arlington, Virginia, USA, 1983, pp. 268–271.
8. F. Mohr, "Thermooptically induced bias drift in fiber optical Sagnac interferometers," J. Lightwave Technol. **14**, 27–41 (1996).
9. E. Quatraro, A. Pizzarulli, M. Catasta, G. Crescenti, E. Spinozzi, M. Zazzetta, and A. Cingolani, "High performance FOG for non-temperature stabilized environment," in *Inertial Sensors and Systems—Symposium Gyro Technology*, Karlsruhe, Germany, 2011, pp. 1.1–1.14.
10. S. Minakuchi, T. Sanada, N. Takeda, S. Mitani, T. Mizutani, Y. Sasaki, and K. Shinozaki, "Thermal strain in lightweight composite fiber-optic gyroscope for space application," J. Lightwave Technol. **33**, 2658–2662 (2015).
11. B. Osunluk, S. Ogut, and E. Ozbay, "Thermally induced bias errors for a fiber coil with practical quadrupole winding," in *IEEE Inertial Sensors and Systems*, Kauai, Hawaii, USA, 2017, pp. 152–155.
12. Z. Zhang and F. Yu, "Analysis for the thermal performance of a modified quadrupolar fiber coil," Opt. Eng. **57**, 017109 (2018).
13. I. A. Esipenko, D. A. Lykov, and O. Y. Smetannikov, "Using the transversely isotropic characteristics of the coil to calculate the thermal-drift parameters of a fiber-optic gyroscope," J. Opt. Technol. **86**, 289–295 (2019).
14. S. Mitani, T. Mizutani, and S. Sakai, "Current status of fiber optic gyro efforts for space applications in Japan," Proc. SPIE **9852**, 985208 (2016).
15. Y. Zhang and Z. Gao, "Fiber optic gyroscope vibration error due to fiber tail length asymmetry based on elastic-optic effect," Opt. Eng. **51**, 124403 (2012).
16. M. Webber, R. Willig, H. Raczkowski, and A. Dineen, "Modeling of rate error in interferometric fiber-optic gyroscopes due to stress induced by moisture diffusion," J. Lightwave Technol. **30**, 2356–2362 (2012).